Fall 2021

Development of a First-Generation Prototype Laboratory System for Rail Neutral Temperature Measurements

Ellie Yi-Hsien Chao

Development of a First-Generation Prototype Laboratory System for Rail Neutral Temperature Measurements

by

Ellie Yi-Hsien Chao

Bachelor of Science
University of South Carolina, 2019

Submitted in Partial Fulfillment of the Requirements

For the Degree of Master of Science in

Civil Engineering

College of Engineering and Computing

University of South Carolina

2022

Accepted by:

Dimitris Rizos, Director of Thesis

Yu Qian, Reader

Michael Sutton, Reader

Robert Mullen, Reader

Tracey L. Weldon, Interim Vice Provost and Dean of the Graduate School

DEDICATION

To my grandfather who passed away unexpectedly from a bike accident. You inspired me to do things I would have never thought of doing. You always believed that I would go beyond and far in life that I never knew I could do.

To my great-grandfather who passed away in 2020, but I was unable to go back to Taiwan to send him off due to COVID restrictions. Thank you all for always believing in me and telling me that I would go far in education.

To my friends for believing and for understanding and being there with me throughout the process.

To my parents and brothers for their unconditional support throughout this whole process. You all were there for me through the good and the bad. Without your constant support, I do not know if I could have even completed this journey.

ACKNOWLEDGEMENTS

I would like to express my thanks and gratitude to the following people. Without their support and guidance, this thesis would not be possible. First, I would like to thank my advisor, Dr. Dimitris Rizos for providing me this research opportunity to complete my M.S. degree. I have learned a lot from you as a mentor and beyond grateful for all the time and energy you have put in in helping me complete this chapter of my life. I would also like to thank Dr. Yu Qian, Dr. Michael Sutton and Dr. Robert Mullen for being a part of the thesis committee and all the additional help and guidance you have provided on this journey. I would also like to thank all the undergraduates that have helped me during laboratory and field testing. I could not have done it with you guys. I would also like to express my sincere thanks to Farzana Yasmeen and the crew at Correlated Solutions, Inc for teaching and guiding me through learning the DIC system from the beginning.

This work has been partially funded by the Federal Railroad Administration (FRA) under contract 693JJ619C000007. The opinions expressed in this article are solely those of the authors and do not represent the opinions of the funding agency.

ABSTRACT

Modern railway tracks worldwide standardize the use of Continuous Welded Rail (CWR) due to its ability to prevent disadvantages associated with rail joints in a track. CWR is laid when the rail is free of thermal stresses, also known as Rail Neutral Temperature (RNT). RNT is controlled in the CWR installation procedure; however, over time, the temperatures deviate from the RNT. The deviation causes significant thermal stresses introduced in the longitudinal direction of the rail, leading to potential failures such as pull-apart and buckling, causing track integrity and safety of train operation. The most significant potential failure is track buckling due to the decrease in RNT over time; therefore, it is important to know the state of stress in the rail at different temperatures and the changes in RNT to maintain the track and prevent track buckling beforehand.

The proposed non-contacting method for this work utilizes stereo vision and 3D Digital Image Correlation (StereoDIC) technology. It is a method that can acquire full-field deformation measurements. The measurements data then can be processed to obtain an RNT estimate and longitudinal stress calculation. Compared to the other existing methods, this method reduces the disadvantages such as system complexity, practicality, reliability, simplicity, and instrumentation demands. Using the novel concept developed from Knopf's work, this paper

furthers provides a preliminary guide for the method's implementation on a full-scale prototype system in the laboratory followed by initial stages for field testing.

TABLE OF CONTENTS

LIST OF TABLES

LIST OF FIGURES

CHAPTER 1

INTRODUCTION

1.1 Background

The history of freight and passenger rail in the United States dates back to the 1700s. Railroad is an essential component of the US transportation network and has played an essential role in the US economy. Freight railroad is the most efficient and economical way to transport commodities (coal, oil, intermodal) long distances. Freight railroads are categorized based on annual operating revenues into three classes, i.e., Class I, Class II, and Class III, as seen in *Table 1.1* [1] [2]. AMTRAK is the only Class I passenger railroad and operates solely long-distance intercity in the continental US.

Table 1.1 Railroad Classification Based on Revenue

Class	Annual Operating Revenue
Class I	Above $900 million
Class II	Between $40.4 million and $900 million
Class III	Less than $40.4 million

The track structure is a critical component of the railroad infrastructure. The most common configuration of a track structure comprises rails, fastened on railroad ties/crossties laying on ballast, while other configurations include slab track and ballastless designs. The rails are typically made from hot-rolled steel and rail size is classified based on weight per linear foot. Typical rail sizes in US railroads are 90RE, 115RE and 132RE. The cross-section is either flat-bottomed or bullhead and is divided into three segments, i.e. head, web, and foot, as shown in

Figure 1.1.

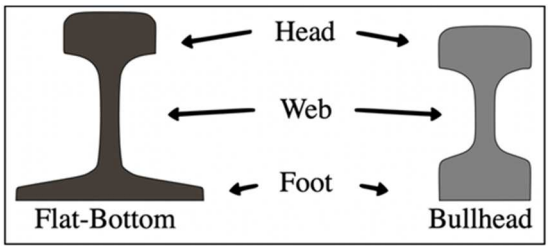

Figure 1.1 Typical rail cross sections

In a ballasted track, rails are attached to the ties through a fastener system. The ties transfer the loads from the rail to the ballast and the subgrade, hold the rails in place and keep them spaced at the correct gauge. Ties are made of wood, concrete, steel, and plastic composite. Majority of the ties are timber ties, but in recent years prestressed concrete ties present a viable alternative. The ballast serves as the foundation of the rail structure, bears the loads from the ties provides lateral support, drains water, and controls vegetation. *Figure* 1.2 shows a typical profile of a ballasted track structure.

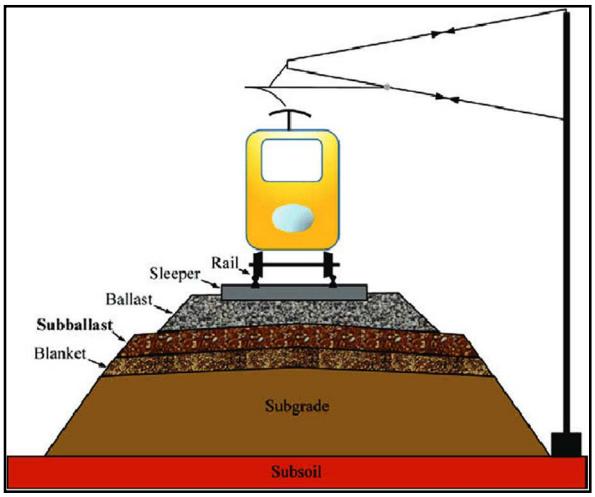

Figure 1.2 Profile of typical ballasted track structure

For a train to run safely and effectively, the rail segments need to join end-to-end to produce a continuous running surface for the train. The traditional method of joining the rails is a connection formed by placing joint bars on the gage and field sides of the rail and bolting through the rail web. A typical bolted joint is shown in *Figure 1.3*.

Figure 1.3 Typical rail joint in jointed track

The bolted connection leaves a small gap between the rail ends creating a discontinuity and an abrupt stiffness change, and they do not offer the best ride quality while accentuating the dynamic effects. Nevertheless, these tracks are still

in use in many countries on lower speed lines and in poorer countries due to the lower construction cost and more straightforward equipment required for installation and maintenance. However, the major problem with using jointed track is the cracking around the bolt holes, which leads to the breaking of the railhead. One major crash known as the Hither Green Rail crash was an incident with 49 casualties and 78 injuries. The crash was caused by derailment from a broken rail. This incident was significant because the British Railways became the first to change from jointed tracks to continuously welded rails [3]. With that, the transition from jointed tracks to continuous welded rail began globally.

1.2 Problem Statement and Objectives of this work

Nowadays, in the US, modern railways use continuous welded rail (CWR). Federal Railroad Administration (FRA) defines CWR as an uninterrupted rail that can run for several miles long by eliminating bolted joints and replacing them with welded connections. Such a joint is shown in *Figure* 1.4. With fewer joints, CWR is stronger, provides a smoother ride, requires less maintenance, and trains can travel on it with higher speeds while having less friction. Because of its advantages, CWR is now the preferable rail to utilize in modern railways.

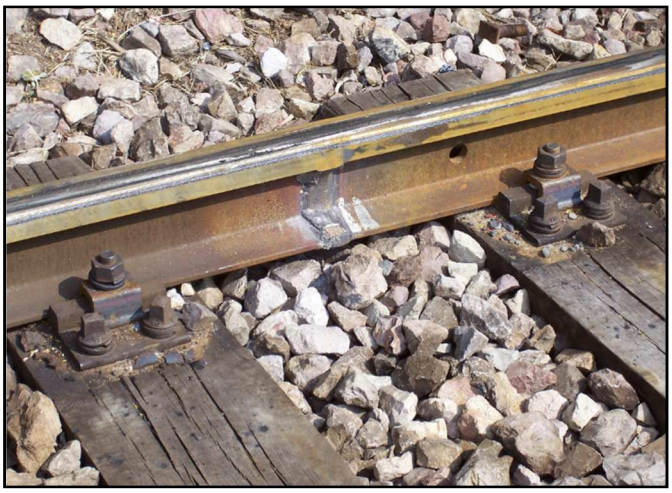

Figure 1.4 Typical flash butt welded joint in CWR

However, the major concern with CWR is the thermal stress that develops in the rail due to the lack of joints. CWR installation is done at a pre-determined temperature typically between 32°C and 43°C to account for regional climate projects to mitigate extreme temperature deviations from the Rail Neutral Temperature (RNT) [4, 5]. RNT is the temperature at the time that the CWR is laid and free of thermal stresses. As temperatures deviate from the RNT, significant tensile or compressive longitudinal stresses develop that can dramatically impact tracks when the steel expands or contracts; it can potentially cause the track to buckle or separate. Buckling is defined as the deformation and displacement of the rail from the original position on the track. That is why the installation procedure is done to prevent the tracks from buckling in the summer or pulling apart in the winter.

Figure 1.5 below shows an example of what buckling would look like in the track.

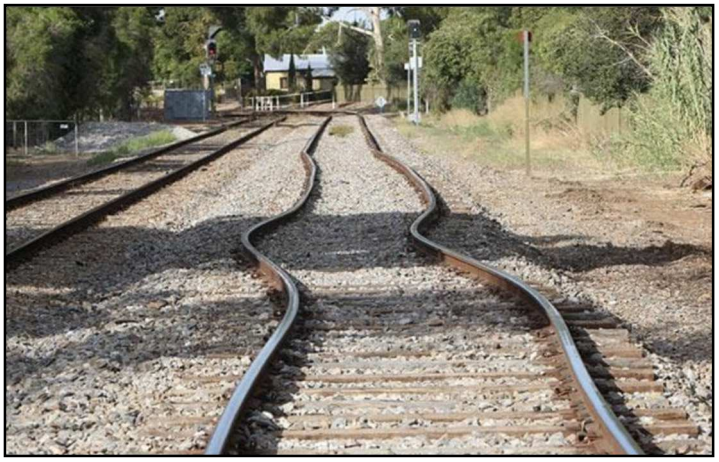

Figure 1.5 Typical track buckling

In North America, the winter cold causes a potential of broken rails, also known as pull-apart. Whereas in the summer heat, it can cause heat kinks which are potentially more hazardous than the broken rails since the current signaling system can detect interruptions due to the broken rails, so no damage occurs. Even though CWR installation procedures control the RNT to preclude buckling under typical seasonal temperature cycles, the RNT of a track segment still generally decreases over time due to factors related to repair, maintenance, shifting of the track structure, track deformations and operating conditions. Thus, it is important to have effective monitoring and prevention methods of RNT as climate projections forecast an increase in average ambient temperatures.

This thesis presents the fundamental concepts for the development of a first-generation prototype laboratory system for RNT measurements. The proposed development is a continuation of Knopf's novel method for estimating RNT and determining longitudinal stress in the rail. Knopf's work proposed a method in which non-uniform deformations can be measured using a non-

contacting vision-based data acquisition system, digital image correlation (DIC), to correlate to the RNT and longitudinal stress in the rail. The method is based on the hypothesis that thermal deformations of the rail in the track are not uniform due to constraints in the longitudinal and transverse directions; therefore, the non-uniform deformations can be correlated to RNT and longitudinal stresses in the rail [4, 5]. The objectives of this thesis are to:

1. Continue the next phases of RNT and longitudinal stress measurement methodology based on Knopf's work
2. Develop a prototype of a vision-based measurement system for laboratory use and field application, etc
3. Investigate speckle patterning techniques that can create the necessary high contrast pattern on the specimen in a most time efficient manner
4. Investigate thermal cameras to adequately assess temperature uniformity and accuracy
5. Additional techniques of heating the specimen to minimize issues with non-uniform heating distributions, the speed of heat dissipation, and limit the heat applied to the supports
6. Investigate field conditions that affect the measurements and define design parameters for next generation prototype for field implementation.

1.3 Thesis Organization

The thesis is organized as the following:

Chapter 1 introduces the rail industry in the US, identifies the problem, and sets the objectives of this work.

Chapter 2 presents the current state of knowledge and discusses how the Digital Image Correlation technology is adopted.

Chapter 3 presents the development of the prototype measurement system.

Chapter 4 implements the prototype measurement system for lab implementations.

Chapter 5 implements the prototype measurement system for field implementations.

Chapter 6 presents the conclusion and provides recommendations for future field implementation.

CHAPTER 2

CURRENT STATE OF KNOWLEDGE IN THE FIELD

This chapter presents the current state of knowledge in RNT measurement methods, stress measurements methods and DIC technologies adopted in this work.

2.1 RNT & Stress Measurements

Several methods technologies have been proposed for estimating the Rail Neutral Temperature and Longitudinal stress measurements; however, there are disadvantages related to each one. The methods can be grouped in respect to the underlying basic principles as:

(i) rail cutting

(ii) rail lifting

(iii) deformation measurements

(iv) ultrasonic

(v) x-ray

(vi) piezoelectric/magnetic

(vii) vibration

(viii) electrical impedance

(ix) mechanical

(x) chemical

(xi) highly nonlinear solitary waves

These basic principles (i) - (viii) are techniques discussed in Knopf's work [4]. Techniques (ix) - (xi) are further summarized in the table below. Table 2.1 is a continuation of Knopf's work that summarizes existing technologies and the associated basic principles and major shortcomings for RNT measurements [4, 5, 6, 7].

Table 2.1 Summary of Methodologies for Measuring RNT

Method	**Basic Principles**	**Shortcomings**
Rail Cutting	Cut rail to release thermal deformations and direct measurement of expansion/contraction	● Time consuming ● Destructive
Rail Lifting	A segment of the rail is unclipped, and the vertical force required to lift the rail is measured. The resistance correlates with rail force and RNT.	● Time consuming ● Semi-destructive ● Cannot be used for rail compression
Deformation Measurements	Uses strain gage, or fiber optics or extensometer data along with rail temperature information to measure rail elongation and establish the part of the temperature	● Instrumentation installation ● Knowledge of thermal strains at time of installation is needed ● Lack of strain variation during normal use

	influence that is present as stress	
Ultrasonic	Sound velocity in the rail is correlated to the stress state	● Sound velocity in a rail free of thermal stresses is required ● Sensitive to material structure and defects ● Requires contact
X-Ray	Distance between two atomic planes in a crystal is measured through X-ray diffraction and related to material stresses	● Measures the stresses in a small volume close to the surface ● Distance data of the atomic planes in various materials at various stress state is needed ● Requires clean surface
Magnetic	Application of alternating magnetic field in the rail produces magnetic noise due to magnetoelastic interaction in ferromagnetic materials. The noise intensity is correlated to the longitudinal stress field in the rail	● Time consuming calibration procedure ● Need measurements from reference material ● Barkhausen noise distribution depends also on microstructure condition of rail material ● Influenced by residual stress
Vibration	Vibration mode characteristics change with the axial force	● Instrumentation installation ● Insufficient accuracy because mode characteristics also depend on track conditions
Electrical Impedance	The PZT first excites the rail to obtain an EMI response signal from the rail that indicates deformation	● Time-consuming instrumentation installation ● Within experimental stages ● Requires contact and power

Mechanical	Beam-Column bending theory to assume that the rail can be schematized as a simply supported beam under concentrated loading to estimate longitudinal stress in the track	● Time consuming ● Cannot be used on curved tracks ● Can only be used to measure RNT when CWR is in tension ● High cost
Chemical	Vibrational spectroscopy technique that measures residual stress in aluminum oxides through exciting the higher energy state by absorption of photonic energy.	● Requires accurate measurements ● early stage of development
Highly nonlinear solitary waves	HNSWs are enabled by a transducer. The transducer consists of a chain of steel particles inside a tube and surmounted by an electromagnet. The electromagnet has a striker that generates a solitary wave pulse that proposes and is dented by the sensor beads or by a force sensor.	● still in development phases

2.2 DIC Technologies

Digital Image Correlation (DIC) is a non-contacting measurement method that uses high-resolution digital cameras to capture sequence of digital images to do imaging analysis of full-field surface displacement and deformation measurement. The sequences of digital images taken are correlated to produce full-field coordinates representations of shape, motion, and deformation of the surface of specimen. The first known form of DIC work was done by Gilbert

Hobrough where the focus was primarily on digitally matching features from two perspective views to extract 3D topography from reconnaissance photographs obtained by a surveillance aircraft back in 1961 [8]. However, the first practical form of DIC started developing in the 1980s. Early studies were focused primarily dealing with mathematical foundations and issues related to scene recognition and reconstruction of stereo image sets [8, 9]. Later studies would further implement the mathematical foundations and converted to digitized 2-D images of planar specimen undergoing in-plane deformations into full-field measurements of displacements [8]. The 2D methodology and implementation of the algorithms by Sutton was preceded with further works of specimen undergoing rigid body motion and a seeded fluid undergoing nominally planar flow [10, 8, 11, 9]. Since the beginning of the fundamental works, 2D-DIC and StereoDIC (3D-DIC) methods have been developed and validated over the past decades and so it is more broadly used in academia, government laboratories and industry [8]. DIC technologies are used worldwide by scientists and investigators seeking to obtain full-field quantitative measurements of motions and deformations in fields such as but not limited to aerospace, automotive, and railway industries [12, 9].

Due to it being a non-contacting measurement method, DIC is independent of the materials being tested, thus wide range of applications are used to investigate and characterize deformation, especially in fields of civil engineering [9, 8]. The stereo-vision DIC demonstrates significant advantages over existing technologies since it is i) a non-contacting system; ii) able to capture full-field

surface deformations; iii) able to acquire highly accurate measurement in the presence of both large rotations and displacements; iv) able to be utilized for both curved and flat surfaces, and v) able to allow for a variable of field of view with the utilization of different lenses [9].

DIC has been used in different aspects of railway applications. Some railway applications include but not limited to [13, 14, 15, 16, 17]

1. DIC in Load Testing and Damage Detection
2. DIC in performance assessment of prestressed concrete railroad ties
3. DIC in ballast and fasteners systems
4. DIC in determining opening stresses for railway steel under low cycle fatigue
5. DIC in monitoring dynamic displacements

These railway applications implementing the use of DIC have shown to be successful in the railway industry.

CHAPTER 3

PROTOTYPE MEASUREMENT SYSTEM DEVELOPMENT

The reference-free, non-contacting concept proposed by Knopf et al. is a promising alternative for measuring the RNT and estimating the longitudinal stress in the rail [4, 5]. The method is based on deformation measurements using stereovision technology and Digital Image Correlation and is furthered developed for implementation. Chapter 3 summarizes the fundamental aspects of the concept introduced in Kopf et al. and defines the data acquisition needs and resources and develops the data processing of a first-generation prototype system for field implementation [4, 5].

3.1 RNT and Stress Measurement Concept

This section summarizes the concept proposed by Rizos and Knopf et al. to the extend required to identify the needs and resources for developing a prototype system [4, 5]. The concept development, verification and validation are presented and discussed in detail in the above cited work. It is noted that the method is a reference-free method

and does not require any prior knowledge of the state of the stress in the rail.

3.1.1 Hypotheses

The RNT and stress measurement concept reported in Rizos and Knopf et al. is based on two main hypotheses [4]:

1. Since the CWR rail is fully constrained in the longitudinal direction, thermal loads will induce non-uniform expansion of the top of the rail in the vertical direction, as shown in Figure 3.1(a)
2. During thermal loading, the web of the CWR rail at a location between two adjacent ties remains stress free in the vertical direction and strain free in the longitudinal, as shown in Figure 3.1 (b).

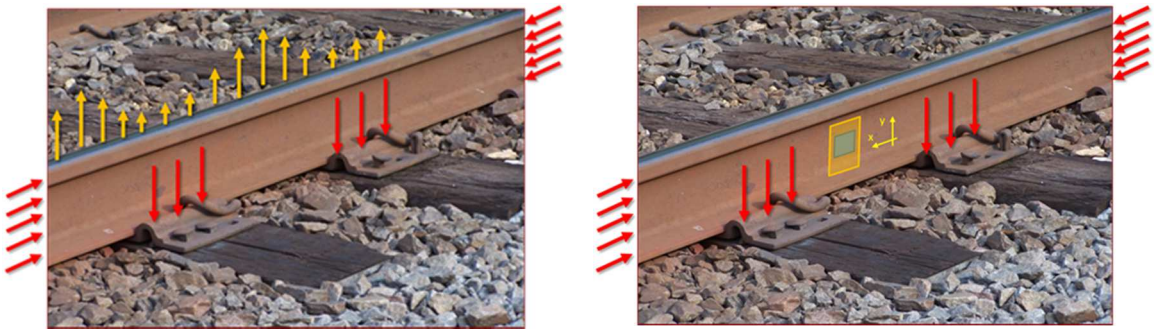

Figure 3.1 Hypotheses of the RNT measurement concept based on rail constraints (red arrows): (a) Non uniform thermal expansion in vertical direction of top of tail shown by orange arrows; (b) Development of negligible strain in the longitudinal direction and significant strain in the vertical.

3.1.2 Concept for Reference Free RNT Measurement

The RNT estimate is computed based on establishing a linear relationship between vertical deformation of the top of rail and temperature known through either naturally occurring or induced thermal cycles. In particular, the curvature of the line defined by the section of the vertical plane with the surface of the rail head (dashed-dot-dot line in Figure 3.2) is computed based on top of rail deformation

measurements at different temperatures. The intercept of the curvature-temperature linear equation is the RNT estimate, implying that when the rail is stress free, the curvature of the line vanishes. Thus, provided that the curvature k_1 and k_2 are computed at two distinct temperatures T_1 and T_2, respectively, the *RNT* is estimated as [4, 5]:

$$RNT = T_2 - k_2\left[\frac{T_2 - T_1}{k_2 - k_1}\right] \quad (1)$$

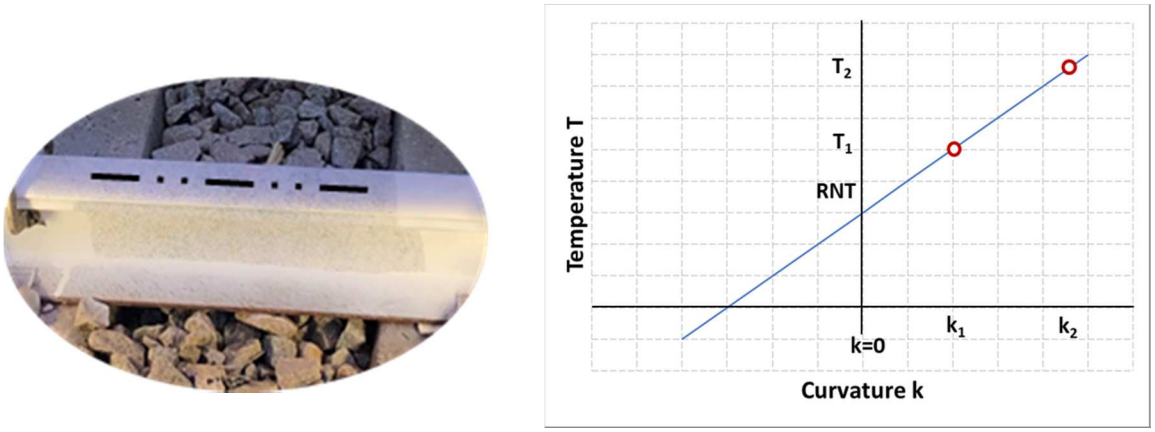

Figure 3.2 Temperature-Curvature relationship and RNT estimate

It is noted that, at any given temperature, the curvature for the top of the rail is uniquely determined from shape measurements without the need of a reference shape.

3.1.3 Concept for Longitudinal Stress Measurement

Once the RNT has been estimated, and in view of the second hypothesis, the change in temperature, ΔT, is correlated to the change in strain, $\Delta\varepsilon_y$, in the vertical direction on the web, as shown in Figure 3.3, and the unique Temperature-Strain linear relationship is established as:

$$T = RNT + \left(\frac{\Delta T}{\Delta \varepsilon_y}\right)\varepsilon_y \tag{2}$$

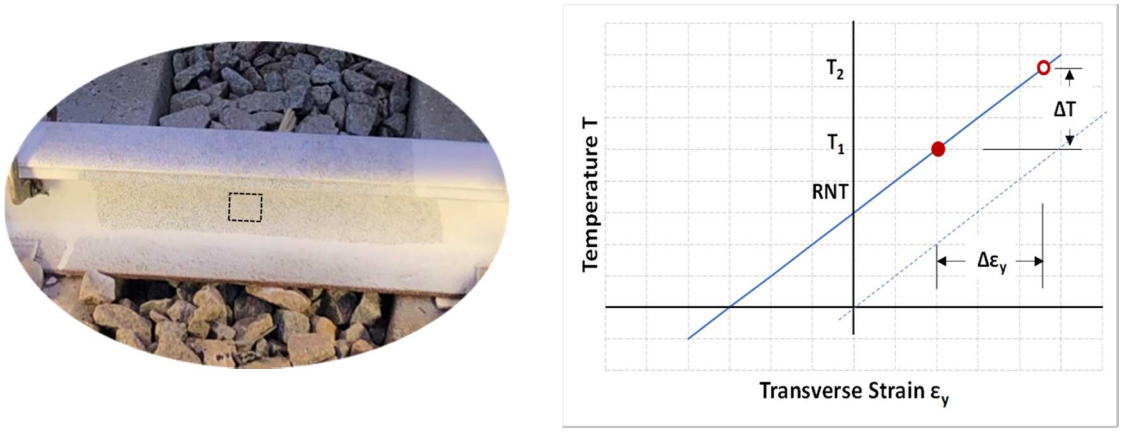

Figure 3.3 Temperature-Vertical strain relationship

Subsequently, the longitudinal stress in the rail is calculated analytically based on the plane stress conditions. It is assumed without loss of generality that there are no initial strains at RNT and the transverse stress σ_y is negligible. Therefore, the longitudinal stress is estimated at any temperature as a function of the measured longitudinal, ε_x, and transverse, ε_y, strain at the web and the material properties as [4, 5]:

$$\sigma_x = (\varepsilon_x - \varepsilon_y)\frac{E}{(1+\upsilon)} + \sigma_y \tag{3}$$

3.2 Prototype System Parameters and Configuration

In view of the RNT measurement concept, the development of a prototype measurement system should account for the features, and address data acquisition needs, discussed in the following sections:

3.2.1 Thermal Loading of Rail

Since a temperature-deformation relationship is sought after, thermal loading and temperature measurements of the rail are necessary. Thermal loading can be achieved either as part of a naturally occurring daily thermal cycle or can be artificially induced through rail heating. Deformation measurements need to be acquired at least at two well separated rail temperatures. It is recommended, however, to acquire deformation measurements at three or more temperatures, to verify the linear temperature-deformation relationships. The minimum required rail temperature separation is 10^{o}F, however, a 20^{o}F is recommended, especially when the testing process involves only a few deformation acquisitions. It is emphasized that the temperature range of the deformation acquisitions does not need to include the RNT. Rail heating needs to be applied in a way to produce a relatively uniform temperature field on the web. It is also important to heat a segment of the rail that is at least five times longer than the center-to-center tie spacing, to fully develop the longitudinal reaction of the rail to the induced thermal expansion.

3.2.2 Hardware for Rail Heating

In this study, the induced temperature cycle approach is implemented for heating the rail. Following experimentation with different options rail heating is induced using silicon heater pads. These flexible pads are selected since they can easily conform to the shape of the rail web and provide full contact for evenly distributed heating. A 3-inch by 70-inch, 120V/1200W *BiSupply* silicone heater pad, shown in Figure 3.4(a) is used**.** To prevent heat loss and increase the heat

transfer efficiency, and to facilitate the installation on the rail, the heating strips are insulated on the control dial side, and the insulated side is attached to 70-inch long 2x4 lumber, as shown in Figure 3.4(b). The heating strip assembly is attached to the gauge side of the rail web surface by using C-clamps. Clamping the heating strip assembly to the gauge side of the web allows the specimen to heat up without interfering with the image acquisition. To ensure that an adequate rail segment is heated, multiple heating strip assemblies can be installed in series.

(a) (b)

Figure 3.4 Rail heating: (a) BiSupply silicone heater pad drum for rail heating (b) Heating strip assembly

3.2.3 Hardware for Rail Temperature Sensing

Thermal imaging is captured during the testing to record the rail temperature and assess the thermal distribution within the FOV of the DIC acquisitions. The thermal scanning is performed using a handheld FLIR E6 Wi-Fi thermal camera, shown in Figure 3.5. The resolution of the infrared sensor is 80 pixels by 60 pixels and the accuracy is +/- 2% of reading for ambient temperature in the range -4^{o}F to 482^{o}F, and object temperature above freezing. These temperature ranges are typical of the testing conditions expected in the field. This lower end thermal camera satisfies the accuracy and resolution needs of the proposed first-generation prototype.

Figure 3.5 FLIR E6 Wi-Fi thermal camera

3.2.4 Deformation Measurements

The proposed RNT measurement concept requires acquisition of deformations in two areas of a rail segment between two consecutive ties, i.e., average curvature along the length of the top surface of the rail head and the strain field on the web. These measurements need to be acquired in high accuracy as demonstrated by the parametric studies reported in Knopf et al [4]. For the minimum temperature separation of 10^{o}F discussed in the preceding section, the expected deformation and strain values are 0.004 inch (0.01 mm) and 130 micro strains, respectively. Thus, any data acquisition with noise less than these values is suitable for the proposed first-generation RNT measurement prototype. The proposed first-generation prototype uses DIC technology to acquire both deformation and strain field measurements. The accuracy of a typical StereoDIC system (10 microns/m FOV and 10$\mu\varepsilon$) is well below the expected values.

3.2.5 DIC System Configuration

The DIC camera system of the proposed prototype consists of two camera pairs, one for the Top-of Rail (TOR) shape and deformation measurements and

the other one for the rail web (WEB) strain measurements. Image acquisition of the TOR and WEB is synchronized and controlled through the image acquisition software.

3.2.5.1 Top of Rail Acquisition

The Top-of-Rail (TOR) images are captured by a pair of “Grasshopper3 USB3” 9.1 MP cameras. The cameras carry the ICX814 imaging sensor, have a physical pixel size of 3.69µm and a camera resolution of 3376 x 2704 pixels. They are paired with identical Tamron 23FM16SP 2/3” high-resolution mono-focal lenses with 16 mm focal length. The minimum required width of the Field of view is the center-to-center spacing of the ties and the midpoint of the rail segment should align with the center of the FOV and clearly marked to be visible on the images. The cameras should be mounted approximately 4 feet above the TOR at an angle between the camera axes in the range 15^{o}-35^{o} and should point straight down on the TOR surface. For focal lenses with length of 16 mm, it is recommended to have a minimum stereo-angle of 25°. The minimum required speckle size is 3 mm.

3.2.5.2 Rail Web Acquisition

The rail web (WEB) images are captured by a pair of “Grasshopper3 USB3” 9.1 MP cameras. The cameras carry the ICX814 imaging sensor, have a physical pixel size of 3.69µm and a camera resolution of 3376 x 2704 pixels. They are paired with identical Kowa LM12HC-SW 1” mono-focal lenses with a focal length of 12.5mm. The minimum required width of the Field of view is the middle third of the spacing of the ties and the midpoint of the rail segment should align with the center of the FOV and clearly marked to be visible on the images. The cameras

should be mounted approximately 4 feet away from the web on the field side at an angle between the camera axes in the range 15º-35º, and a focal point at the midpoint of the rail segment between two consecutive ties. For focal lenses with length of 12.5 mm, it is recommended to have a minimum stereo-angle of 35°. The minimum required speckle size is 3 mm.

3.2.5.3 Camera System Calibration

Once the camera systems are set up, the system needs to be calibrated to obtain the geometric and transformation parameters for each camera that will allow to establish an accurate image scale. Image scale refers to the number of pixels in the image corresponding to a specific physical distance on the physical specimen and accounts for hardware feature and lens distortion corrections. Calibration is based on a calibration target, shown in Figure 3.6 consisting of known diameter dots arranged in a rectangular array. The size of the calibration target depends on the size of the field of view. In this study, the maximum width of the FOV is approximately 30” and two calibration targets of 12x9 dots spaced at 18 mm, or 25 mm on center may be used. A coordinate system is defined by three hollow fiducial dots included in the rectangular array.

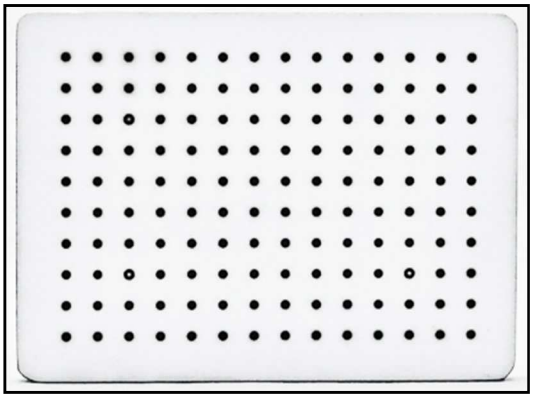

Figure 3.6 An example of a 12x9 calibration target

3.2.5.4 Lighting

Image acquisition for DIC requires adequate illumination of the specimen. Natural light, although a preferred option, may not always serve the purpose, especially in field measurements where moving shadows on the specimen due to the sun's motion relative to the horizon create varying and abrupt contrast changes. Thus, controlled lighting conditions may be necessary. In this work, three low-heat emission light sources, shown in Figure 3.7 are used:

(i) Four Bi-color 500 Ultra Bright LED Studio Light Panel – 9M-01LED009-500-07. These fixtures are dimmable LED arrays mount on dedicated tripods and have been mostly used in a laboratory setup.

(ii) Four Nanlite LITOLITE-28F 5600K LED Fresnel fixtures. Each light produces 1960 lumens from an LED array, are dimmable and focusable, and feature 5600K color temperature to blend with ambient daylight. These fixtures are mounted directly on the mounting frame shown in Figure 3.8.

(iii) One CSI 1050 LED Light Kit. The light kit comes with two magic positioning arms, one LED driver with on/off switch, one power supply

with power cable and two linear polarizers. These light fixtures are equipped with MR16 LED bulbs – LUMR16CL 6W/12V. Each light produces about 450 lumens and a beam angle of around 38 degrees. These lights are used exclusively in field measurements to eliminate effects of shadows. They must be used with polarized blue filter lenses.

Figure 3.7 Light Sources for DIC applications: (a) Studio LED Array, (b) Focusable LED; and (c) Blue light sources.

3.2.5.5 Camera Mounting

The first configuration of the camera mounting system used dedicated tripods for each of the camera systems. Although this configuration was adequate for preliminary investigations and laboratory environments and facilitated individual camera position adjustment, its setup was very inefficient and time consuming. The next design consists of a single tripod supporting a bracket frame that carries the camera systems on slider bars. This system maintained the advantage of individual camera position adjustment and improved the setup process and time. However, this system was unstable when used in the field. The latest design is a portable aluminum frame that is adjustable, supports the camera systems and lighting and is shown in Figure 3.8

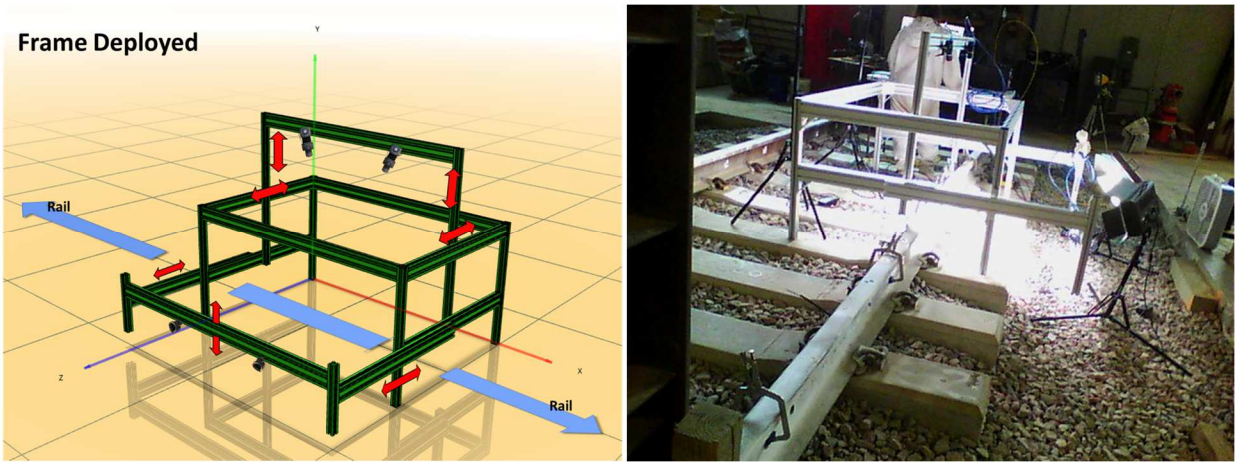

(a) (b)

Figure 3.8 Aluminum frame for mounting of DIC systems: (a) Frame design; (b) As built and in service

3.2.5.6 Software

For image acquisition and processing, the commercial software used is VIC-Snap 9 and VIC-3D 8, respectively. VIC Snap-9 is the application used to acquire images for the work done in this paper. VIC-3D 8 is used for image processing through DIC to calculate full field shape, deformation, and strains.

3.3 General Testing Procedure Steps

The following testing methodologies are the general procedures that are applicable to both in lab and field testing. A general description for each process is also included as recommendations and guidance.

1. Clean rail surfaces. Rail surfaces are cleaned using wire brushes attached to an electric drill. The surface is grinded to remove any imperfections for a smooth, and clean surface for speckling.

2. Apply white paint (matte finish). Flat white spray paint is used on the surface of where speckle patten will be done. The paint must adhere adequately to the test piece and should be of uniform thickness.

3. Apply speckled pattern by stamp and roller. Speckle pattern must have a good pattern that consists of a random, isotropic, high contrast, consistent speckle and 50% coverage. The stamp is inked on a stamp pad with black ink and “stamped” onto the top of the rail. It is recommended to stamp the top of the rail twice to get good coverage. For the web, the roller is used. The roller is inked on the stamp pad as well and “rolled” onto the side of the web. It is recommended to go through the passes at least three times for a good coverage. It is important to note that one should not go through the passes until the dots have dried to prevent smearing.

4. Attach heating strip(s). Depending on area of heating, the heating strips are attached to the back of the rail. To secure the heating strips, C clamps are used to hold it in place.

5. Set camera systems, lights and calibrate. Cameras and lights are setup properly and then calibrated to ensure the system is ready for testing.

6. Acquire baseline images (Set0). Baseline images are taken to use as a reference point during data processing.

7. Record ambient and surface temperatures. All temperatures are acquired by using the FLIR E4 handheld thermal camera. Temperatures are recorded in a lab form.

8. Start heating cycle. The heating cycle starts when all heating strip(s) are turned on and heats up the rail.

9. Every 10^{o} F (approximately) acquire image and temperature measurements. At every 10°F increments, data acquisition will be done. DIC images will be taken, and temperature recordings will be taken with the handheld thermal cameras for both the top of the rail and the web. All temperature recordings will be noted in the lab form.

10. At ~140^{o} F remove heating strips and begin cooling cycle. At the maximum temperature, approximately 140°F, the heating strip will be powered off, unclamped, and removed from the rail. The rail will then be cooled down with a typical fan to approximately 100°F.

11. Every 10^{o} F (approximately) acquire images and temperature measurements. At every 10°F increments, data acquisition will be done. DIC images will be taken, and temperature recordings will be taken with the handheld thermal cameras for both the top of the rail and the web. All temperature recordings will be noted in the lab form.

12. Recalibrate systems to cross check system parameters. At the end of the heating and cooling, the system is to be calibrated again to cross check the system parameters. This is to ensure there were no movement of the system during the testing.

3.4 Data and Image Processing

After the system images and temperature measurements are collected, the data measurements need to be processed. The collected images will convert into measurement data and then applied to the proposed RNT measurement method to calculate RNT. The following explains how the DIC images are processed into RNT measurement.

1) Significance of projection error - Projection error, also known as epipolar error, measures how well the correlation results agree with the stereo calibration. It is a good indication for possible drift, misalignment, or vibrations in the camera/lens systems. There is no single, fixed threshold for projection error to separate “good” from “bad” calibrations; however, there is a direct relationship between errors and errors in DIC measurements. The rule of thumb for projection is that is should typically be on the order of the calibration score. The cause of error should be investigated the more significantly larger the projection error is in comparison to the calibration error.
2) Criteria for selecting subset and step - Subset size is defined as the width and height of subset square in reference. Whereas step size is the distance between subset centers. The units for them are in terms of units of pixels. The idea subset size should contain at least three speckles but not more than seven speckles. For this study, the approximate subset size is about 35-45 pixels for the FOV. The typical step size that is recommended is one-third to one-half of the subset size so that the neighboring subsets partially

overlap. In VIC-3D 8, there is a suggested subset size function that will help identify a suggested subsize size based on the selected AOI.

3) Measurement Extraction - The software performs the image correlation by tracking the speckle pattern in a sequence of images. The software recognizes each local variation in image intensity as a “feature”. To extract the measurements from the software, the features are identified and accurately located in the image. The software then measures the pixels in each image. The physical pixel sizes vary from camera to camera. The most common way to estimate the motions of the features is to select a subset in the initial image that contains sufficient pixels with high contrast to match the speckle pattern in the deformed image so accurately determine the motion. The selected subset has blocks of pixels, so the software searches the following sequence of images captured during motion/deformation to find corresponding pixels with the same intensity pattern. From there the subset center is ascertained in the reference image from which displacement will then be calculated. For stereo-DIC the out of plane algorithm is measured using the triangulation approach. Since each DIC point is a vector, the displacement is measured in the software as U, V and W, in terms of pixels. The subset in the deformed images is compared to the subset of the reference to find the displacement measurements on the surface of material. The surface measurements calculated from the software can then be extracted.

4) Curve fitting - With the extracted surface measurements from the DIC software, an EXCEl spreadsheet is designed to capture the out-of-plane displacement measurements to do curve fitting for the data. The spreadsheet takes the x and z directions, defined in the software, and does least square approximation for fitting the quadratic polynomial. The mathematical approach used for Visual Basic Application (VBA) code for EXCEL is based on the matrix formulation as:

$$\begin{bmatrix} n & \sum_{i=1}^{n} x_i & \sum_{i=1}^{n} x_i^2 \\ \sum_{i=1}^{n} x_i & \sum_{i=1}^{n} x_i^2 & \sum_{i=1}^{n} x_i^3 \\ \sum_{i=1}^{n} x_i^2 & \sum_{i=1}^{n} x_i^3 & \sum_{i=1}^{n} x_i^4 \end{bmatrix} \begin{bmatrix} A \\ B \\ C \end{bmatrix} = \begin{bmatrix} \sum_{i=1}^{n} y_i \\ \sum_{i=1}^{n} x_i y_i \\ \sum_{i=1}^{n} x_i^2 y_i \end{bmatrix} \quad (4)$$

Using the matrix, the variables A, B and C are solved. The coefficients A, B and C are used in the quadratic equation as:

$$y = Ax^2 + Bx + C \quad (5)$$

The code will run through the calculation above for all data sets, n, and then generate the quadratic curve for each number of data sets, n. From there an average of the curve will be collected and curve fitting and linear regressions will apply. Based on the gauge length the user defines, to derive the curvature calculation, the plots will be generated within the specified area of interest. For this study the RNT measurement is found

within the middle third of tie-to-tie spacing. From the linear regression of the average curvature deformation, the RNT measurement is calculated.

CHAPTER 4

LAB IMPLEMENTATION

This chapter showcases the implementation of the RNT measurement method done in the laboratory. A series of laboratory testing for the proposed track system were constructed and conducted in the University of South Carolina (USC) Railway Testing Center. The testing conducted is categorized into two categories: preliminary testing and full-scale track rail system implementation.

4.1 Objectives

The objective for the lab implementations is to prepare the measurement method to be practical and easy for field implementations. The goal for the lab implementation is to also streamline a general procedure for field testing.

4.2 General Testing Materials

A variety of materials are needed and necessary to collect measurement data. The materials needed for testing are categorized into the following:

1. DIC system – this includes any software and technology needed to perform the DIC such as DIC stereo cameras, computer, and commercial licenses, etc.
2. Speckle Patterning - this includes any items needed to apply speckle pattern on the specimen such as flat white spray paint, stamps and rollers, sharpies, and acetone, etc.
3. Extension Cords – this includes any outlets or extension cords to allow for multiple power source during testing
4. Lighting Needs – this includes any lighting fixtures and supplies to provide for the right needed lighting on the specimen such as light fixtures, polarized lenses, and blue lights, etc.
5. Miscellaneous - this includes any items and tools that may be used to secure or clean during testing such as pliers, drills, sledgehammers, and zip ties, etc.

4.3 General Testing Procedure Steps

The following methodology is the general procedures taken for lab testing. The procedures are a generalized, guided process for acquiring DIC measurements.

1. Prepare rail specimen for testing including cleaning, surfacing and speckle patterning
2. Set up, zero and calibrate LVDT sensors to measure displacement
3. Set up DIC camera systems, lights and calibrate system
4. Attach heating strips to specimen, without heating strips on

5. Acquire baseline images
6. Start heating cycle
    - Acquire images and temperature measurements at approximately every 10°F
    - Record ambient and surface temperatures at every data set
7. Heat up approximately 140°F and remove heating strips
8. Begin cooling cycle
    - Remove and power off heating strips to cool down the rail; use a fan t
    - Acquire images and temperature measurements at approximately every 10°F
    - Record ambient and surface temperatures at every data set
9. Cool down to approximately 100°F
10. Recalibrate system to cross check system parameters

4.4 Observations and Lessons Learned

From the lab implementations, observations and lessons were learned regarding speckle details, lighting needs, displacement accuracy, handheld thermal camera accuracy and calibration needs.

4.4.1 Speckle details

Improper speckle pattern can cause inconsistencies in the surface measurements. One important aspect of speckle pattern is the speckle density. Without the right amount of speckle density, the subset sizes will be relatively

large. Lighting can help subset sizing to a certain degree, but speckle density is the main criteria. Speckle patching refers to only patching portions of the speckle pattern when there are bad speckles. For this study when doing speckle patching, there will be surface differences which will cause the curvature deformation to not be correctly calculated. *Figure 4.1* shows the impact of speckle patching has on the surface measurement.

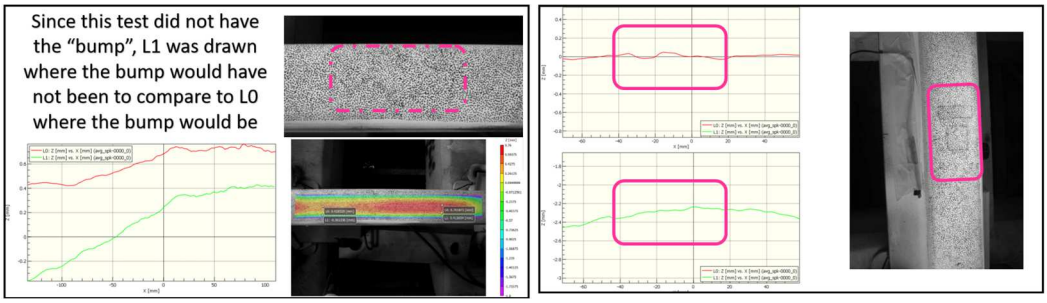

Figure 4.1 Impact of speckle patching on surface deformations

Another problem that can cause surface deformation measurements to be incorrect is speckle pattern not adhering properly to the specimen surface. If the specimen surface is rigid and not smooth, then the deformation calculations gathered from the data acquisition will be inaccurate because it is not the closest to the specimen surface. Just like the specimen surface needs to be smoothen out, the paint used for speckle patterning cannot be 1) too smooth, 2) not uniformly disturbed and 3) too thick. When the paint has any of the three issues mentioned, then the data acquisition measurements will cause skewed data collection. The spray paint should be spray at a distance that is not too close to the specimen or else the paint will be too thick. Before spraying it is recommended to shake the spray can well so that the paint does not clump up and spray somewhere that is

not the area of interest to ensure that the paint has been mixed well and ready for usage.

4.4.2 Lighting needs

Lighting is an important aspect to capturing data for analysis. Without the proper lighting data collected can be hard to analyze. It is important to not have too much lighting because that can cause reflection but not having enough lighting can cause the image to be too dark for the software to process the data. With the proper amount of lighting the subset size will be better. Since the cameras and speckle pattern can cause reflections, lighting needs to be set up so that it is ideal to both situations. When outside, a lighting fixture may not be necessary and instead may need to filter out the natural light with either reflectors and/or polarized lenses.

4.4.3 Displacement accuracy

The LVDT sensors connected to the end of the track during testing were able to collect the displacements at each data acquisition set. The average displacement for each set was compared to the displacement collected from the stereo-DIC. The displacements collected from the stereo-DIC is relatively close to the average displacements collected from the LVDT sensors.

4.4.4 Thermal Sensing Equipment

The FLIR E6 Wifi thermal camera is backchecked with a FLIR SC6700 Long Wave infrared camera to see if the handheld FLIR E6 is sufficient for field testing. The handheld IR camera has a resolution of 10,800 pixels and a frame rate of 9

Hz, whereas the Long Wave has a resolution of 327,680 pixels and a programmable frame rate of 0.0015 Hz to 125 Hz. The long wave infrared camera is seen in Figure 4.2. It can be seen that the camera is larger in size which is not convenient for field testing.

Figure 4.2 FLIR SC6700 long wave infrared camera

Through comparing the two infrared cameras it is seen that the temperatures are in close readings, shown in *Figure 4.3*.; therefore, there is no need to use the FLIR SC6700 in the field and is sufficient for capturing thermal readings.

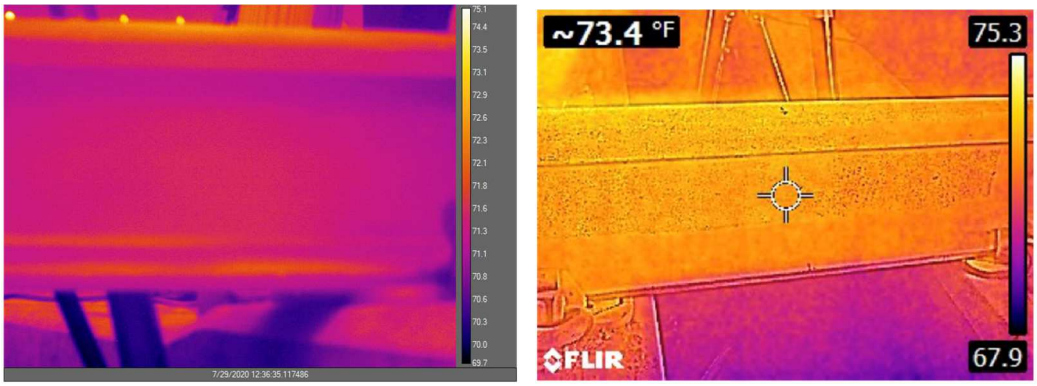

(a) (b)

Figure 4.3 Infrared thermal camera temperature reading comparison: (a) FLIR SC6700 Long Wave temperature reading (b) FLIR E6 Wifi thermal camera reading

4.4.5 Calibration needs

Selecting the proper calibration grid size is important because it can issue with calibration parameter and transformation of the system. It is important to remember that when selecting calibration grid size that the grid needs to fill up approximately 2/3 of the area camera frame. *Figure 4.4* shows an example of a wrong calibration target size being used causing inaccurate data. In the figure the actual distance is measured to be 5inches from the midpoint of FOV to the edge of the support but from the software it is seem that 5inches from the midpoint is not to the edge of the tie. The cause of this error is due to the grid size used was too small causing a bad calibration.

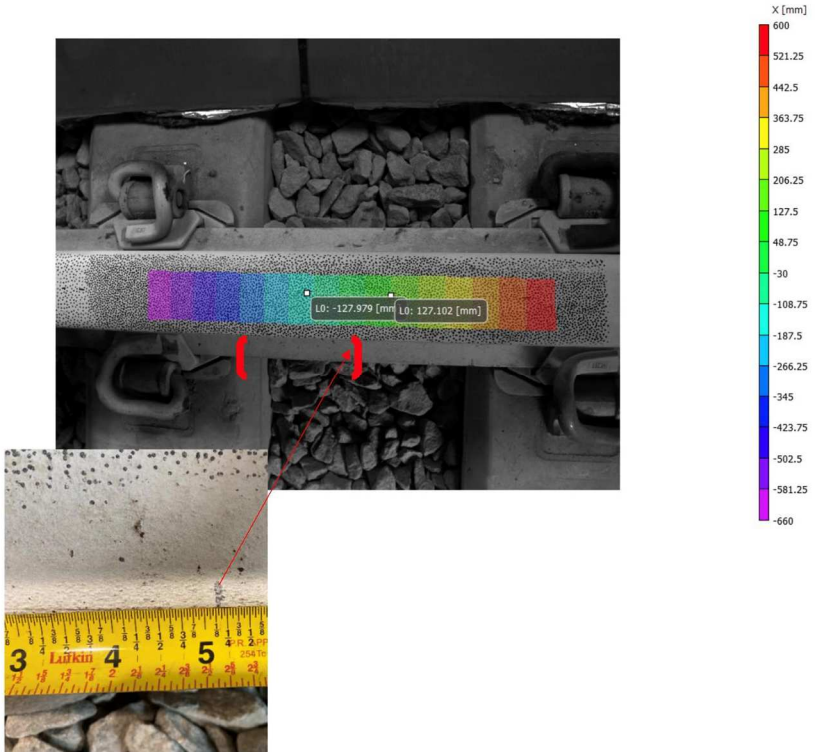

Figure 4.4 Inaccurate data collected due to inaccurate calibration grid selected

4.5 Discussion of Results and Conclusion

From the results there is no correlation in RNT due to the welding imperfections of the rail causing the rail to not have the needed full constraint at the ends. However, the objective of the lab implementation is to streamline a procedure and learn from the testing to see what needed to be perfected in preparation for the field.

CHAPTER 5

FIELD IMPLEMENTATION

The prototype RNT measurement system, as developed in Chapter 3, is implemented in the field with the objectives to investigate the effects of field conditions on the measurements and to identify weaknesses and areas of improvement in both the hardware and the test process. Three sites have been selected: (i) the SC Railroad Museum (SCRM) in Winnsboro, South Carolina; (ii) the CSX track near Wade, North Carolina and (iii) the CSX track at Alpine Rd in Columbia, South Carolina. Figure 5.1 shows the three locations on a Google Map.

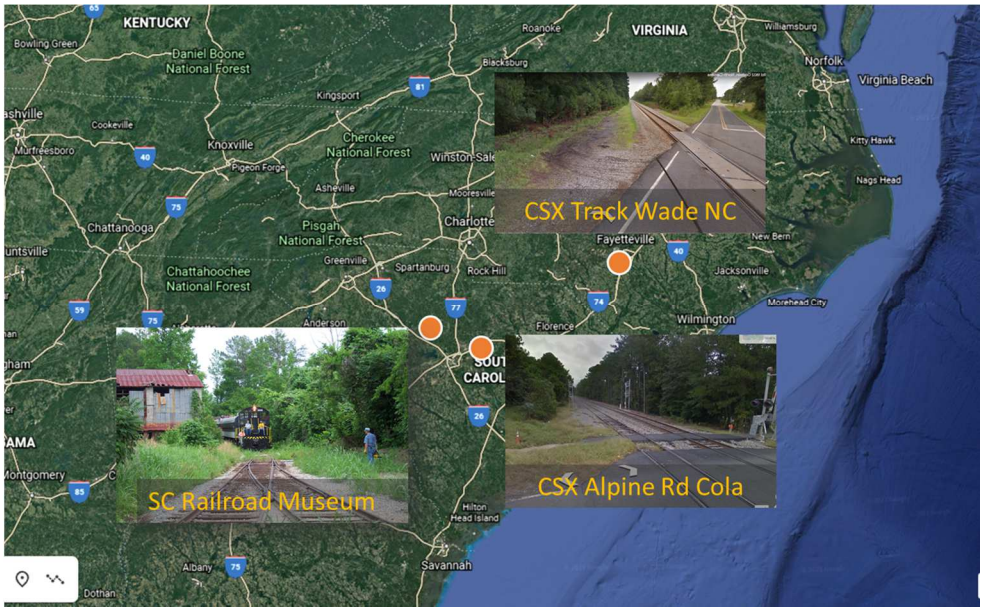

Figure 5.1 Locations of field implementation sites

5.1 Concrete Tie Jointed Track (Non-CWR Track) – SC Railroad Museum

The SC State Railroad Museum (SCRM) is in Winnsboro, SC. The railroad museum is the center for historic trains of the Rockton, Rion & Western Railroad, with rides displays and charter. It operates exclusively for educational and scientific purposes. The track in the SC Railroad Museum is a jointed rail track on concrete ties and is shown in Figure 5.1 . Typical rail segments are 39 feet long. The South Carolina state railroad museum test took place in May 2020. It represents the first attempt to implement the proposed RNT and stress measurements methodology in the field. The objective of this field study is to get an initial understanding of field conditions. Since the SCRM track is not a CWR track a direct validation of the RNT measurement is not expected. However, in the absence of the longitudinal rail constraints, the temperature and the TOR should not be correlated.


Figure 5.2 SC railroad museum track

For field experimentation, the procedures are like the lab implementation procedures. The differences are that the lighting fixture is different due to the natural sunlight, and no loading is applied. The procedures for the field testing are discussed in the following sections.

5.1.1 Rail Preparation and System Setup

The speckle pattern is applied on both the TOR and the rail web. The rail surfaces in the Area of Interest (AOI) to be speckled required a light brushing and cleaning to remove any loose rust particles. The areas are first coated with a white flat paint to create a non-reflective background surface that will be in high contrast with the black speckles. Once the white coat is dry, approximately fifteen minutes, the speckle is applied manually dot-by-dot using a black sharpie. After all point is dried, the heating strips are attached on the gauge side of the rail web.

Two separate stereo-DIC systems are used in this test: one for the TOR measurements and another one for the web. Each system is supported by its own

tripod and controlled by its own dedicated computer. Image acquisition of each system is independent of the other, and only an approximate synchronization of the acquisition is achieved. Each system is calibrated independent of the other using a 12x9 18 mm calibration target. The calibration parameters for the TOR and Web camera systems are shown in *Table 5.1* and Table 5.2, respectively.

Table 5.1 Calibration Parameters of TOR Camera System

TOR System		
Camera 1 Type: Pinhole Center x: 1697.69 pixel Center y: 1384.04 pixel Focal length x: 4370.73 pixel Focal length y: 4370.73 pixel Skew: 0 Kappa 1: -0.172405 Kappa 2: 0.855978 Avg.mag.: 8.14154 pixel/mm Min.mag.: 7.4963 pixel/mm Max.mag.:9.06931 pixel/mm	Camera 1 Type: Pinhole Center x: 1692.62 pixel Center y: 1358.05 pixel Focal length x: 4371.11 pixel Focal length y: 4371.11 pixel Skew: 0 Kappa 1: -0.170529 Kappa 2: 0.823742 Avg.mag.: 8.21664 pixel/mm Min.mag.: 7.53702 pixel/mm Max.mag.:9.29301 pixel/mm	Transformation Alpha: 0.0811138 deg Beta: -15.6517 deg Gamma: 0.183031 deg Tx: 173.536 mm Ty: -0.72185 mm Tz: 19.1666 mm Baseline: 174.593 mm

Table 5.2 Calibration Parameters for Web Camera System

Web System		
Camera 1 Type: Pinhole Center x: 1683.86 pixel Center y: 1377.11 pixel Focal length x: 3457.66 pixel Focal length y: 3457.66 pixel Skew: 0 Kappa 1: -0.175236 Kappa 2: 0.0705645 Avg.mag.: 3.95753 pixel/mm Min.mag.: 3.78836 pixel/mm Max.mag.:4.14262pixel/mm	Camera 2 Type: Pinhole Center x: 1705.05 pixel Center y: 1384.6 pixel Focal length x: 3465.22 pixel Focal length y: 3456.22 pixel Skew: 0 Kappa 1: -0.201897 Kappa 2: 0.197565 Avg.mag.: 3.79368 pixel/mm Min.mag.: 3.59154 pixel/mm Max.mag.:4.00597 pixel/mm	Transformation Alpha: 0583435 deg Beta: 15.8673 deg Gamma: 0.395604 deg Tx: -317.594 mm Ty: -1.81563 mm Tz: 45.3174 mm Baseline: 320.816mm

5.1.2 Testing Procedure and Image Acquisition

Once the systems are set and calibrated, an initial set of image pairs are acquired by each system and the thermal image of the AOI of the rail and the adjacent rail is captured. Subsequently, the heating phase initiates, and the rail temperature is monitored. During the heating phase, image sets for each system are acquired in approximately 10^{o}F temperature increments, as measured at the rail web. Once the rail temperature reaches 150^{o}F, the thermal strips are removed, and the rail is allowed to cool down naturally. Due to the sun exposure and the higher ambient temperature the rail temperature does not return to the temperature at the beginning of the test. During the cool-down phase, image sets for each system are also acquired in approximately 10^{o}F temperature decrements, as measured at the rail web. At the end of the test the camera systems are recalibrated. It is noted that during image acquisition, due to the sun's position constantly changing, moving shadows were observed on the AOI and it was necessary to cast a temporary shade over the AOI.

5.1.3 Image Processing and Results Interpretation

The acquired images for the TOR and rail web were used in DIC analysis for the TOR deformations and rail web strains, respectively. The images at the beginning of the induced heating cycle were used as the baseline images and the corresponding temperature was recorded as 76^{o}F. The profile of the TOR is computed at each temperature and the quadratic polynomial is fitted to the data. Figure 5.3 shows the TOR profiles at the baseline temperature and at temperature T=116^{o}F. The solid lines show the profiles where the rail irregularity is evident,

while the dashed lines show the quadratic polynomial fit for computing the average curvature in each case.

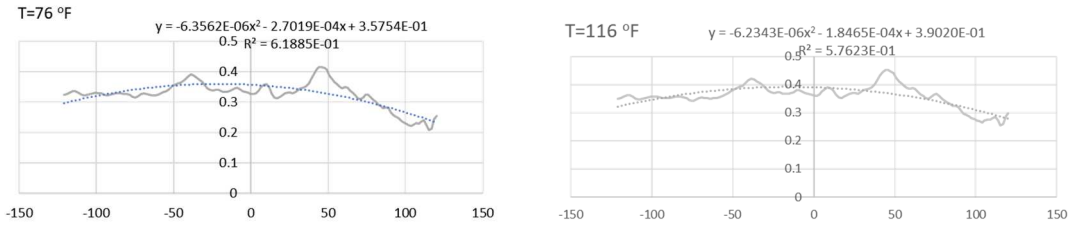

(a) (b)

Figure 5.3 TOR profile and quadratic fit at: (a) T=76 °F and (b) T=116 °F

The Temperature-Curvature relation is shown in Figure 5.4(a), where, as expected, curvature does not change with temperature increase since the SCRM track is not a CWR. Further evidence is shown in Figure 5.4(b) that shows the change in the longitudinal and vertical strain as temperature changes. In this case it is observed that the strain increases uniformly in both directions indicating that the rail expands freely, and, thus, there are no longitudinal constraints. It is also observed, however, that during the initial 20-degree temperature change, the longitudinal strain is negligible compared to the vertical strain, indicating a possible constraint due to friction between the rail and tie plate. However, this observation requires further investigation that is beyond the scope of this thesis.

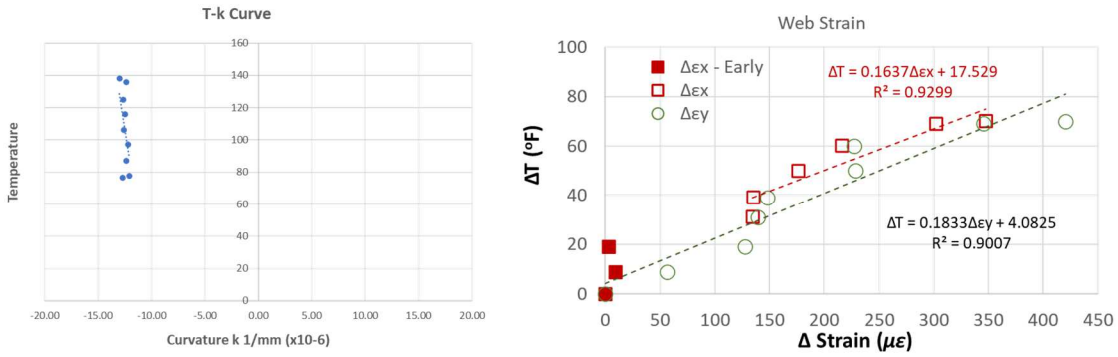

(a) (b)

Figure 5.4 (a) Temperature-Curvature relationship; (b) Temperature Change vs. Strain Change

5.1.4 Observations

Upon arrival to the site at 8:45 am, the rail temperature is relatively uniform. However, direct exposure to natural sunlight heats the rail quickly. Therefore, by the time the speckle pattern and setup were complete (approximately 1:00 pm) the rail temperature had reached 114°F. However, the rail under the tent, where the testing AOI is located, is distinctively cooler than the area outside the tent and allowed for the first image acquisition to take place at a temperature of 76°F. With the thermal heating strip, the rail was able to reach a temperature of 146°F. Figure 5.5 below shows the highest temperature reached from natural heating (left image) and thermal-induced heating (right image). Furthermore, speckle application by hand is very time-consuming and challenging due to the extremely limited working area and tight space.

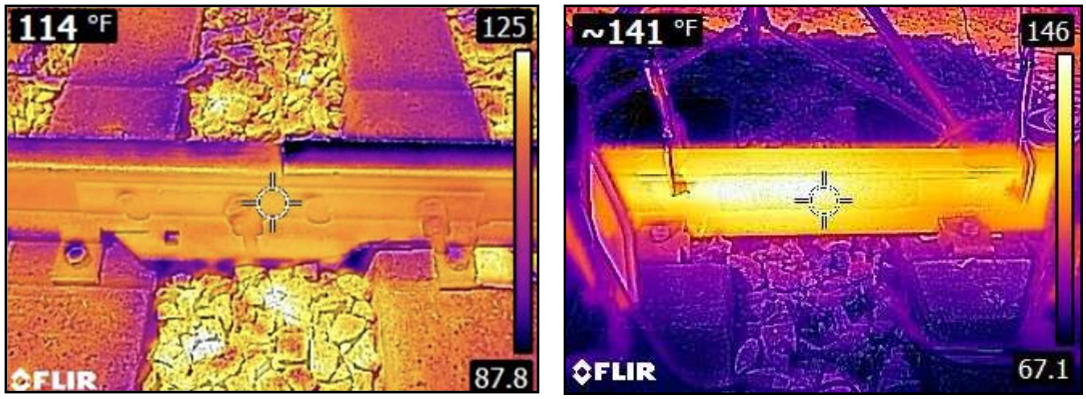

Figure 5.5 Rail temperature at the beginning of the test (left picture) and the end of the heating cycle (right picture)

5.2 Concrete Tie CWR Track – CSX Wade, NC

The next site is a CSX track in Wade, NC and is the first field study where the proposed prototype is implemented in a CWR track. The Wade site is a CWR track on concrete ties with a desired RNT 110^{o}F and is shown in Figure 5.6. The objectives of this field study are to: (a) identify effects of field conditions on testing procedure, (b) validate the proposed protype RNT and (c) guide modification and enhancements to improve the efficiency of the testing procedure. Testing was conducted at three separate times, i.e., November 2020 (Test 1), April 2021 (Test 2) and June 2021 (Test 3).

Figure 5.6 CSX Track in Wade, NC

5.2.1 Rail Preparation and System Setup

The AOI for Test 1 and Test 3 is approximately 22 inches, slightly larger than the tie spacing, while it was increased to 34 inches in test 2. The speckle pattern is applied on both the TOR and the rail web. The rail surfaces in the Area of Interest (AOI) to be speckled required a light brushing and cleaning to remove any loose rust particles. The areas are first coated with a white flat paint to create a non-reflective background surface that will be in high contrast with the black speckles. Once the white coat is dry, approximately fifteen minutes, the speckle is applied by a stamp and/or roller. After all point is dried, the heating strips are attached on the gauge side of the rail web. The heating length was 60 inches in Test 1 and Test 3, and 180 inches in Test 2.

A single stereo-DIC system is used in Test 1, as shown in Figure 5.7(a). The system is first set and calibrated for web strain measurements during the heating phase of the thermally induced cycle. At the end of the heating phase, temperature was maintained in the rail, while the stereo-DIC system is repositioned and calibrated for TOR measurements. Subsequently, the heating strips were removed, and images of the TOR were acquired while the rail was cooling down. In Test 2, a single tripod is modified and equipped with aluminum extrusions to carry both systems in a two-in-one configuration, as shown in Figure 5.7(b). In test 3, a new fully adjustable frame is designed to carry both systems, as shown in Figure 5.7(c). Both camera systems are controlled by a single computer and TOR and the acquisition of the images is synchronized through software. Each system is calibrated independent of the other using a 12x9 25 mm calibration target.

(a) (b) (c)

Figure 5.7 Camera system support: (a) One-in-One tripod; (b) Two-in-One tripod (c) Custom made, adjustable, support frame.

5.2.2 Testing Procedure and Image Acquisition

Once the systems are set and calibrated, an initial set of image pairs are acquired by each system and the thermal image of the AOI of the rail and the adjacent rail is captured. The rail temperature at the beginning of the heating phase was recorded as 66.7°F, 90.5 °F, and 92.8 °F in Test 1, 2, and 3, respectively. Subsequently, the heating phase initiates, and the rail temperature is monitored. During the heating phase, image sets for each system are acquired in approximately 10°F temperature increments, as measured at the rail web. Once the rail temperature reaches approximately 130°F, the thermal strips are removed, and the rail is allowed to cool down naturally. At the end of the test the camera systems are recalibrated. It is noted that during image acquisition, due to the sun's position constantly changing, moving shadows were observed on the AOI. To mitigate these effects, a canopy was used in Test 2 to create a shade over the entire testing area during the entire test while a light diffuser/sun blocker was used in Test 3 to cast a shade over the AOI only during image acquisition.

5.2.3 Image Processing and Results Interpretation

The acquired images for the TOR and rail web were used in DIC analysis for the TOR deformations and rail web strains, respectively. The images at the beginning of the induced heating cycle were used as the baseline images and the corresponding temperature was recorded. The profile of the TOR is computed at each temperature and the quadratic polynomial is fitted to the data. In all three tests, the average curvature of the top of the rail changes with curvature. This relationship is shown in Figure 5.8, where the linear correlation is evident. The intercept of temperature-curvature relation is the RNT estimate. All three tests predicted an RNT within 3°F of the desired 110°F RNT temperature.

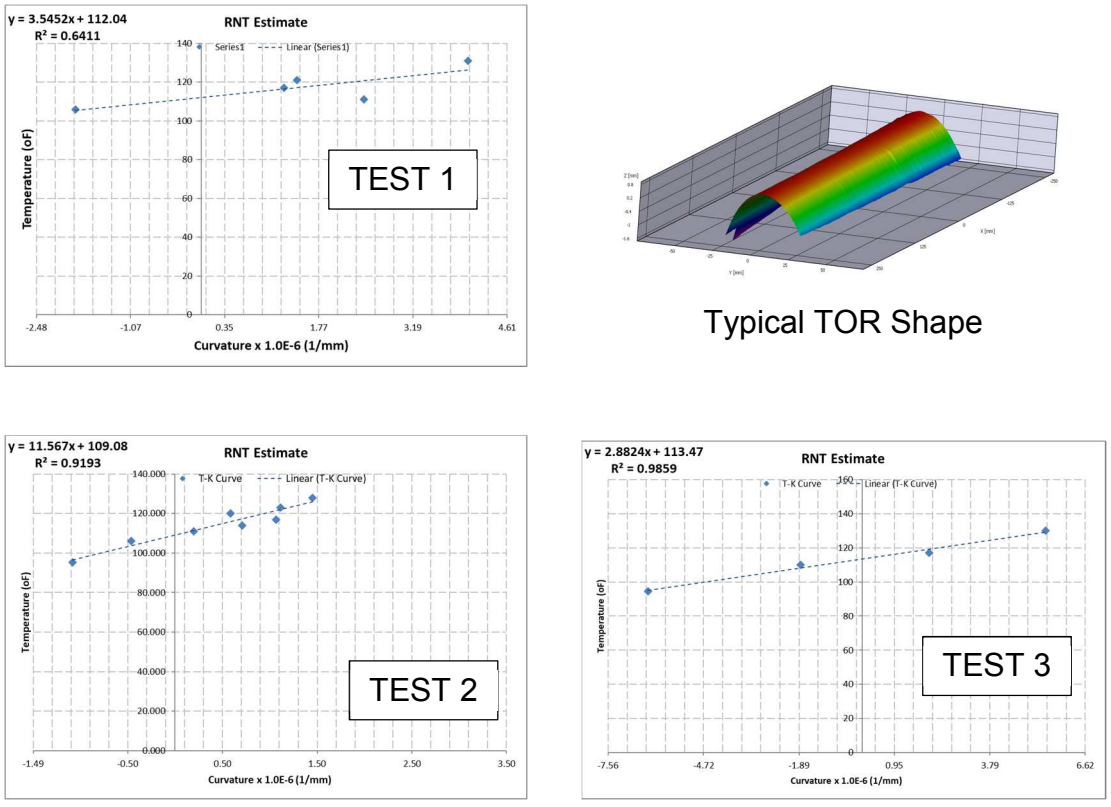

Figure 5.8 Temperature-Curvature relation for three tests and RNT estimate

The web strains in the longitudinal and vertical directions as temperature changes are shown in Figure 5.9. It is observed that in both cases the longitudinal strain is less than the vertical strain indicating some degree of rail constraint in the longitudinal direction due to the CWR action. In particular, when a longer rail segment is heated, i.e. Test 2, the longitudinal strain becomes negligible compared to the vertical direction, as expected.

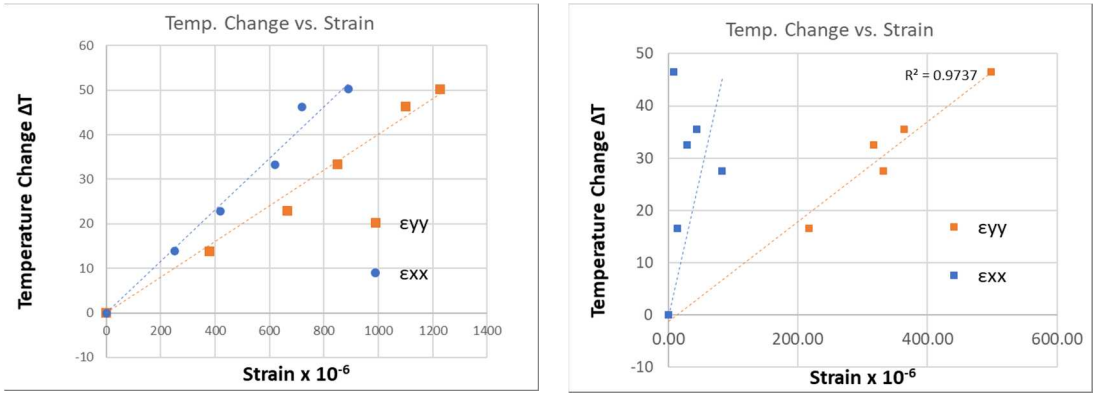

(a) (b)

Figure 5.9 Temperature Change vs. Strain Change: (a) Heated length 60 inch; (b) 180 inch

5.2.4 Observations

This test represents the first successful implementation of proposed technology in the field. The RNT is estimated are within 3°F of the desired 110°F RNT temperature, while the assumptions of linear temperature-curvature and temperature-strain relationship is valid. It is recommended, however, to start earlier in the morning to take advantage of cooler temperatures. Not using canopy for shade causes reflections, varying intensity, and color saturations. Using polarized lenses alone to eliminate sun effects helps but do not solve the problem.

5.3 Timber Tie CWR Track – CSX Columbia SC

The next site is a CSX track in Columbia, SC and is the first field study where the proposed prototype is implemented in a CWR track on timber tie. The Columbia site is a RE115 CWR track on timber ties with a desired RNT 105^{o}F and is shown in Figure 5.10. The objectives of this field study are to: (a) identify effects of field conditions on testing procedure, (b) validate the proposed protype RNT on timber track and (c) guide modification and enhancements to improve the efficiency of the testing procedure. Testing was conducted in September 2021.

Figure 5.10 CSX Track in Columbia, SC

5.3.1 Rail Preparation and System Setup

The AOI is 22 inches, slightly larger than the tie spacing. The speckle pattern is applied on both the TOR and the rail web. The rail surfaces in the Area of Interest (AOI) to be speckled required a light brushing and cleaning to remove any loose rust particles. The areas are first coated with a white flat paint to create a non-reflective background surface that will be in high contrast with the black speckles. Once the white coat is dry, approximately fifteen minutes, the speckle is applied manually dot-by-dot using a black sharpie in Test 1, while it was applied by a stamp and/or roller in Test 2 and Test 3. After all point is dried, the heating strips are

attached on the gauge side of the rail web. The heating length was 120 inches in this test. It is noted that a third heating strip could not be installed since it interfered with one of the rail anchors.

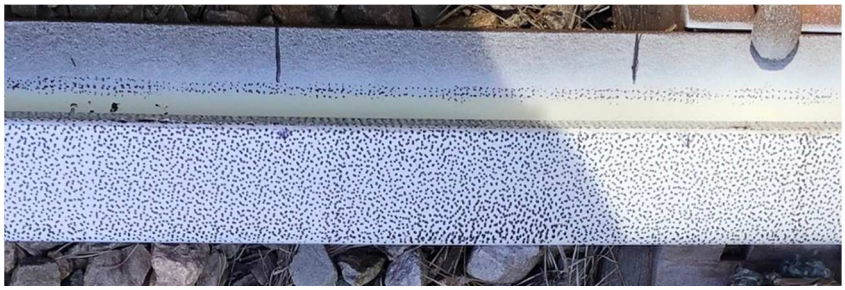
(a)


(b)

Figure 5.11 Speckle as applied at the (a) TOR and the (b) WEB

In this test, the fully adjustable frame, shown in Figure 5.7(c), carries both systems. Both camera systems are controlled by a single computer and TOR and the acquisition of the images is synchronized through software. Each system is calibrated independent of the other using a 12x9 25 mm calibration target.

5.3.2 Testing Procedure and Image Acquisition

Once the systems are set and calibrated, an initial set of image pairs are acquired by each system and the thermal image of the AOI of the rail and the adjacent rail is captured. The rail temperature at the beginning of the heating phase was recorded as 80.8^{o}F. Subsequently, the heating phase initiates, and the rail

temperature is monitored. During the heating phase, image sets for each system are acquired in approximately 10^{o}F temperature increments, as measured at the rail web. Once the rail temperature reaches approximately 130^{o}F, the thermal strips are removed, and the rail is allowed to cool down naturally. At the end of the test the camera systems are recalibrated. It is noted that during image acquisition, due to the sun's position constantly changing, moving shadows were observed on the AOI. To mitigate these effects, a sun blocker was used during image acquisition.

5.3.3 Image Processing and Results Interpretation

The acquired images for the TOR and rail web were used in DIC analysis for the TOR deformations and rail web strains, respectively. The images at the beginning of the induced heating cycle were used as the baseline images and the corresponding temperature was recorded. The profile of the TOR is computed at each temperature and the quadratic polynomial is fitted to the data. In all three tests, the average curvature of the top of the rail changes with curvature. This relationship is shown in Figure 5.12 where the linear correlation is evident. The intercept of temperature-curvature relation is the RNT estimate. The test predicted an RNT within 2^{o}F of the desired 105^{o}F RNT temperature.

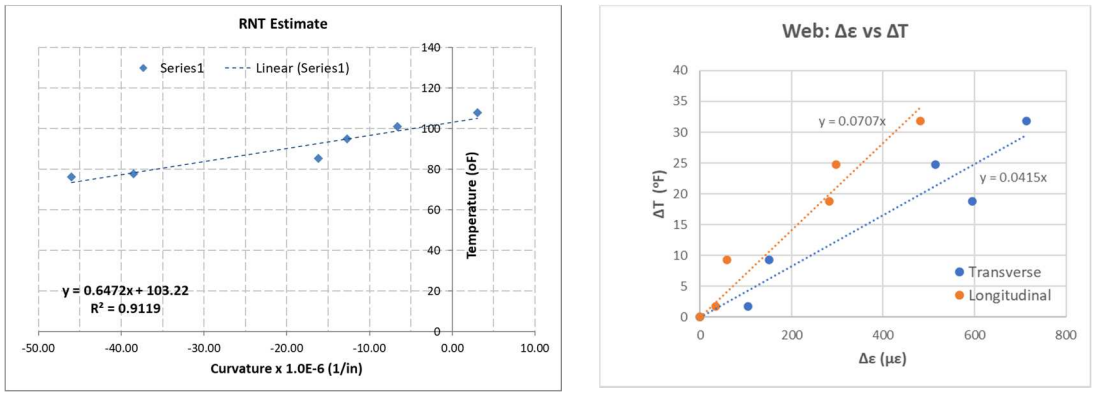

(a) (b)

Figure 5.12 Timber track test: (a) Temperature-curvature relation; (b) Temperature-strain relation

The web strains in the longitudinal and vertical directions as temperature changes are shown in Figure 5.12. It is observed that in both cases the longitudinal strain is less than the vertical strain indicating some degree of rail constraint in the longitudinal direction due to the CWR action.

5.3.4 Observations

This test represents a successful implementation of proposed technology in the field. The RNT is estimated are within 2ºF of the desired 105ºF RNT temperature, while the assumptions of linear temperature-curvature and temperature-strain relationship is valid. It is recommended, however, to start earlier in the morning to take advantage of cooler temperatures. Not using canopy for shade causes reflections, varying intensity, and color saturations. Using polarized lenses alone to eliminate sun effects helps but do not solve the problem.

5.4 Summary of Findings

From the different testing completed in the field, the tests show that the proposed technology is a successful implementation in the field. The RNT estimate are within 2^{o}F to 3^{o}F of the desired RNT temperature. From the field implementations, it is recommended to start early morning when there is no sun. With the sun coming in, the shade from the sun can cause reflections, and even with using polarized lenses to eliminate sun effects, it cannot eliminate the problem.

CHAPTER 6

CONCLUSIONS AND FUTURE IMPLEMENTATIONS

6.1 Conclusions

This thesis presents a method that discusses the feasibility to continue the development of the non-contacting, reference-free measurement system to set the foundations for the design of a full-scale practice prototype. Knopf's thesis's proposed system and method are developed to estimate the RNT and the longitudinal rail state of stress. This study is done through preliminary laboratory testing, full-scale track system implementation, and field testing. These findings serve as a guide for the fundamentals for further field testing and a practical field prototype system. In addition, these preliminary studies investigated the effects of different variables on the stereo-DIC calibration system and its effects on the measurement data.

Upon the completion of this work, the following conclusions can be made:

- The most critical parameter is the level of longitudinal constraint at the rail ends or the vertical constraint at the tie supports. The rail ends must be fully constrained to induce the local flexure along the rail properly. Due to imperfections in welding causing improper constraint at the rail ends, the RNT estimate, and longitudinal strains are not accurate; however, the field testing shows that the method successfully works.

- There are successful findings in the proposed methodology. The deflection profiles are used that estimate an RNT within ±3% error of the pre-defined RNT.
- Even with polarized lenses, sunlight cannot be eliminated. A sunshade helps with the sun reflections, varying intensities, and color saturations. It is better to start field testing early to avoid problems with the sun.

6.2 Future Implementations

While this thesis successfully demonstrates the feasibility of the proposed system, this is only the second phase of a multi-phase project. This work only provides a preliminary guide for future implementation of this method for field testing. The recommendations made for future work include:

- Calibrate FE models with experimental data from field and laboratory testing
- Investigate alternate methods of ensuring complete longitudinal constraint at the rail ends to ensure the full-scale system is fully constrained and not only partially constrained for the laboratory
- Investigate in better adhesives for implementing the adhesive sticker speckle pattern method
- Investigate RNT difference in the field for consecutive crossties and its impact on rail length

REFERENCES

[1] US Government, "Economic Data," [Online]. Available: https://prod.stb.gov/reports-data/economic-data/.

[2] Surface Transportation Board, "Economic Data," 2019. [Online]. Available: https://www.stb.gov/reports-data/economic-data/.

[3] M. o. Transport, "Report on the Derailment that occured on 5th November, 1967 near Hither Green," London, 1968.

[4] K. Knopf, "A Non-Contacting System for Rail Neutral Temperature and Stress Measurements," Masters of Science Thesis, Columbia , 2019.

[5] K. Knopf, D. C. Rizos, Y. Qian and M. Sutton, "A non-contacting system for rail neutral temperature and stress measurements: Concept development," *Structural Health Monitoring,* vol. 20, no. 1, pp. 84-100, 2021.

[6] A. Enshaeian and P. Rizzo, "Stability of continuous welded rails: A state of the art review of structural modeling and nondestructive evaluation," *Journal of Rail and Rapid Transit ,* 2020.

[7] R. Zhang, H. Wu and C. Yang, "Non-destructive Technologies for Stress-Free Temperature Measurement of Continuous Welded Rails," *Vibration Engineering for a Sustainable Future,* pp. 245-251, 2021.

[8] M. A. Sutton, F. Matta, D. Rizos, R. Ghorbani, S. Rajan, D. H. Mollenhauer, H. W. Schreier and A. O. Lasprilla, "Recent Progress in Digital Image Correlation: Background and Developments since the 2013 W M Murray Lecture," *Experimental Mechanics,* vol. 57, no. 1, pp. 1-30, 2017.

[9] M. A. Sutton, J.-J. Orteu and H. W. Schreier, Image Correlation for Shape, Motion, and Deformation Measurements Basic Concepts, Theory and Applications, Springer, 2009.

[10] W. H. Peters III, W. F. Ranson, M. A. Sutton, T. C. Chu and J. Anderson, "Application of digital correlation methods to rigid body mechanics," *Opt Eng,* vol. 22, no. 6, pp. 738-743, 1983.

[11] M. A. Sutton, W. J. Wolters, W. H. Peters III, W. F. Ranson and S. R. McNeil, "Determination of displacements using an improved digital correlation method," *Image Vis Comput,* vol. 1, no. 3, pp. 1333-1339, 1983.

[12] M. A. Sutton, "Image-based Measurements in Solid Mechanics: A Brief History, Static and Dynamic Application Examples and Recent Development," 2014.

[13] A. H. Abdulqader, "Product Qualification and Performance Assessment of HSRM Prestressed Concrete Railroad Ties through Laboratory Testing," 2017.

[14] C. A. Murray, A. W. Take and N. A. Hoult, "Measurement of veritcal and longitudinal rail displacements using digital image correlation," *Candian Geotechnical Journal,* vol. 52, no. 2, pp. 141-155, 2015.

[15] A. A. Rashid, R. Imran and M. Y. Khalid, "Deteremination of opening stresses for railway steel under low cycle fatigue using digital image correlation," *Theoretical and Applied Fracture Mechanics,* vol. 108, 2020.

[16] D. C. Rizos, ""Remote Sensing" Techniques for Railway Infrastructure Monitoring," 2020.

[17] D. C. Rizos, "High Strength Reduced Modulus Concrete for Railroad Crossties," 2017.

[18] P. Reu, "The Art and Application of DIC Introduction to Digital Image Correlation: Best Practices and Applications," *Society for Experimental Mechanics Experimental Techniques ,* 2012.

[19] P. Reu, "The Art and Application of DIC Hidden Components of DIC: Calibration and Shape Function - Part 1," *Society for Experimental Mechanics Experimental Techniques,* 2012.

[20] P. Reu, "The Art and Application of DIC Hidden Components of 3D-DIC: Triangulation and Post Processing - Part 3," *Society for Experimental Mechanicals Experimental Techniques,* 2014.

[21] P. Reu, "The Art and Application of DIC All About Speckles: Speckle Size Measurements," *Society for Experimental Mechanicals Experimental Techniques,* 2014.

[22] K. DeGood, "Understanding Amtrak and the Importance of Passenger Rail in the United States," 4 June 2015. [Online]. Available: https://www.americanprogress.org/issues/economy/reports/2015/06/04/114298/understanding-amtrak-and-the-importance-of-passenger-rail-in-the-united-states/.

[23] Standardization, Good Practices, and Uncertainty Quantification Committee, "A Good Practices Guide for Digital Image Correlation," *International Digital Image Correlation Society,* pp. 1-110, 2018.

[24] Correlated Solutions, Inc, "The VIC-EDU System," 2021. [Online]. Available: https://www.correlatedsolutions.com/vic-edu/.